Novel Antenna-in-Package Design in LTCC for Single-Chip RF Transceivers

Y. P. Zhang, M. Sun, and W. Lin

***Abstract*—An antenna-in-package (AiP) design offers an elegant antenna solution to modern single-chip RF transceivers. The AiP design that integrates an antenna or antennas with a single-chip RF transceiver die into a standard surface mounted device represents an innovative and important development in the miniaturization of radio systems in recent years. In this paper, we present a novel AiP design in low temperature cofired ceramic (LTCC) technology for single-chip RF transceivers operating in the 5-GHz band. First, we focus on the design of a microstrip line antenna on an LTCC substrate. Then, a double-resonance technique and a meshed ground plane are proposed to enhance the impedance bandwidth of the microstrip line antenna. Next, the microstrip line antenna is integrated into the novel AiP with emphasis on feeding the microstrip line antenna using the packaging elements of the carried single-chip RF transceiver die. After that, a unique AiP design which supports the operation of differential signal to suit the mainstream design of single-chip RF transceivers in a differential architecture is described. Finally, the performance of the original AiP design is verified by experimental results.**

***Index Terms*—Chip antennas, low temperature cofired ceramic (LTCC) technology, wireless communications.**

I. INTRODUCTION

RECENTLY, single-chip RF transceivers in CMOS technology for wireless LAN applications in the 5-GHz band have been successfully demonstrated [1], [2]. Single-chip RF transceivers have the benefit of cost reduction and system reliability and therefore represent the trend for implementing radio systems for wireless communications. An antenna is a key component of an RF transceiver because it affects the performance of the RF transceiver as a whole. The antenna appears currently impossible to be integrated into a single-chip RF transceiver for efficient radiation at 5 GHz. Consequently, it is left external to the chip (or chips) in virtually all solutions of highly integrated radio systems.

To provide single-chip RF transceivers with proper antennas, the antenna industry has developed various chip antenna solutions [3], [4]. All these chip antennas employ dielectric loading techniques to miniaturize their size [5]. The dielectric materials are often ceramics with high permittivity and LTCC technology is widely used for manufacturing chip antennas in large quantities [6]. These chip antennas are physically small but they are discrete and need to be assembled with single-chip RF transceivers on printed circuit boards. The area occupied by a chip antenna on a circuit board impedes further miniaturization of the radio system.

To overcome the problems of chip antenna solutions and to better match with single-chip RF transceivers, an elegant antenna solution, that is, integration of an antenna or antennas on/in a chip package that carries the single-chip RF transceiver has been recently proposed [7]–[13]. An antenna realized in this manner is now known as an antenna-in-package (AiP) [13]. The first AiP was demonstrated in a ceramic package [7]. The influences of the carried single-chip RF transceiver die on the antenna performance of the AiP are analyzed in [8]. The different physical parts of the cavity-up ceramic ball grid array (CBGA) package are characterized to optimize the AiP in [9]. The concurrent dual-band operation of the AiP is investigated in [10]. The circuit model of the AiP is derived in [11] for codesign purposes. The codesign of power amplifiers with the AiP is discussed in [12].

It should be mentioned that there have been some important works similar to AiP for multichip solutions of RF transceivers. They are implemented in plastic packages [14]–[16] or ceramic packages [17], [18]. The typical designs also include a novel RF front end package featuring a parasitic antenna in [19] and a hollow dielectric resonator antenna as a packaging cover in [20]. The designs in plastic packages have a cost advantage over those in ceramic packages.

An AiP often uses a microstrip patch or a planar inverted-F antenna [7]–[12], [14], [15], [17], [18]. It has been realized that the microstrip patch and the planar inverted-F antenna cause micro fractures or warpage to the AiP if no additional process steps such as post firing in LTCC are adopted [6]. In other words, use of a microstrip patch or a planar inverted-F antenna as well as a solid ground plane in an AiP should be avoided from the mechanical perspective. In this paper, we present a microstrip line antenna with a meshed ground plane that has both good electrical and mechanical properties and particularly suits AiP fabrication in LTCC. The theoretical design is described in Section II. The integration of the microstrip line antenna into the AiP is detailed in Section III, with an emphasis on feeding the antenna from the carried single-chip RF transceiver die using the packaging elements. AiP design to support the use of differential signals is highlighted in Section IV, which suits the mainstream design of single-chip RF transceivers in a differential architecture. The experimental results of the AiP designs are discussed in Section V. Finally, the conclusion is drawn in Section VI.

Manuscript received June 22, 2007; revised March 10, 2008. Published July 7, 2008 (projected).

Y. P. Zhang and M. Sun are with the Integrated Systems Research Lab, School of Electrical and Electronic Engineering, Nanyang Technological University, Singapore 639798, Singapore (e-mail: eypzhang@ntu.edu.sg; sunmei@ntu.edu.sg).

W. Lin is with Fretune Communication Technology Ltd., Shanghai, China (e-mail:linwei@fretune.com).

Color versions of one or more of the figures in this paper are available online at http://ieeexplore.ieee.org.

Digital Object Identifier 10.1109/TAP.2008.924706

0018-926X/$25.00 © 2008 IEEE

Authorized licensed use limited to: Nanyang Technological University. Downloaded on February 25,2010 at 22:03:30 EST from IEEE Xplore. Restrictions apply.

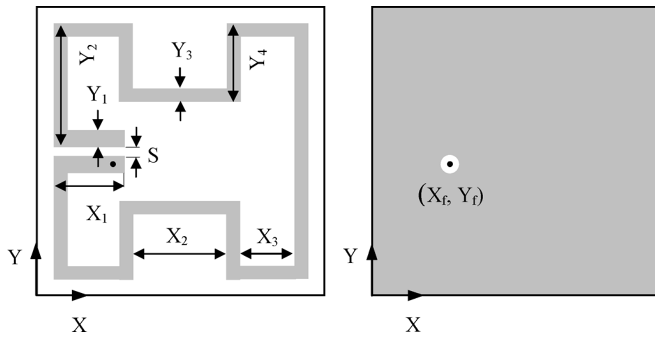

Fig. 1. Top and bottom views of the basic structure of the microstrip line antenna.

TABLE I
DESIGN PARAMETERS OF THE MICROSTRIP ANTENNA

Parameters	Basic structure	Double Resonance	Meshed ground plane
X_1	3.98	3.98	3.98
X_2	6	6	6
X_3	2.44	2.44	2.44
X_4	-	4.2	4.2
X_5	-	-	0.25
X_6	-	-	0.55
S	0.3	0.3	0.3
Y_1	1.52	1.52	1.52
Y_2	7.85	7.85	7.85
Y_3	1.28	1.28	1.28
Y_4	5.2	5.2/5.4*	5.4/5.22*
X_f	3.98	3.98	3.98
Y_f	7.3	7.3	7.3

Dimension in mm, * optimized value

II. MICROSTRIP LINE ANTENNA

The antenna for an AiP should be scalable for operating at different frequencies and trimable for adjusting the accuracy of the resonant frequency. Scalability shortens the design cycle, while trimability greatly improves the production yield. The microstrip patch and the planar inverted-F antenna used in early AiP designs meet these requirements. However, as previously stated, they have potential to cause mechanical problems to the AiP. In this section, we describe the theoretical design of the microstrip line antenna and the meshed ground plane that has both good electrical and mechanical properties and particularly suit the AiP fabrication in LTCC for operating at frequencies below 10 GHz.

A. Basic Structure

Fig. 1 shows the basic structure of the microstrip line antenna. As shown, the line radiating element is printed on the top surface of a substrate with a ground plane on the bottom. The substrate material is LTCC with a dielectric constant of 7.8 and a loss tangent of 0.002. The metal material is silver with a conductivity of 5.7 $\times 10^8$ $\mathrm{S/m}$. The metal thickness is 10 $\mu\mathrm{m}$. Note that the line radiating element is excited with a via through a circular aperture in the ground plane. Its length can be easily scaled and shaped to operate at different frequencies and its gaps or corners can be trimmed with laser to fine-tune the resonant frequency.

Extensive parametric studies using the HFSS have been conducted to design the antenna. They reveal that the length and width of the line radiating element should be chosen between $1.3 \sim 1.5\lambda_{\mathrm{o}}$ and between $0.03 \sim 0.05\lambda_{\mathrm{o}}$, respectively where λ_{o} is the free space wavelength. The matching to a 50-Ω source can be achieved by properly adjusting the width Y_1 and the gap S. The resonant frequency can be tuned only by adjusting the length Y_4. A longer Y_4 corresponds to a lower resonant frequency.

The microstrip line antenna excited with a single feed can be considered as a meandered monopole antenna. The bends and their separations as arranged in Fig. 1 force the current on the Y-directional line sections to flow along the same direction thus producing strong radiation, while force current on the X-directional line sections to flow along the opposite directions thus generating weak radiation. As a result, a linearly-polarized radiation is achieved.

The targeted antenna operating frequency is 5.775 GHz for the IEEE 802.11a standard in a body size of $17 \times 17 \times 0.8\ \mathrm{mm}^3$. The height of the substrate $h = 0.8\ \mathrm{mm}$ is chosen by a guideline $h \leq \lambda_0/(4\sqrt{\varepsilon_{\mathrm{r}} - 1})$ to avoid the excitation of the TE1 mode surface wave and to have sufficient mechanical strength [21]. The antenna design parameters are listed in Table I. Fig. 2(a) shows the simulated input impedance. It is seen that the antenna resonates at 5.775 GHz. Fig. 2(b) shows the simulated return loss. The antenna impedance bandwidth is 50 MHz from 5.755 to 5.805 GHz. The narrow impedance bandwidth is due to the thin substrate and high dielectric constant. Fig. 2(c) and (d) shows the simulated radiation patterns in the E- and H-planes at 5.775 GHz, respectively. It is seen that the antenna radiation patterns are similar to those of a microstrip patch antenna on a small ground plane. The simulated peak gain and radiation efficiency at 5.775 GHz are 4.7 dBi and 80%, respectively.

B. Double Resonance

To broaden the narrow impedance bandwidth of the basic structure, the double-resonance technique is used. The second resonance is created by adding another current path as shown in Fig. 3.

Using the design parameters listed in Table I, we simulated the antenna performance. It is observed from Fig. 4(a) that with the initial $\mathrm{Y}_4 = 5.2\ \mathrm{mm}$ the second current path results in the double resonances at 5.825 and 5.875 GHz. The antenna impedance bandwidth is thus enhanced to 80 MHz (5.795–5.875 GHz) as shown in Fig. 4(b). However, the operating frequency shifts away from 5.775 GHz. To shift back the operating frequency, it is found that increasing the length X_4 is not as effective as increasing the length Y_4. This is because the length X_4 mainly affects the second resonance, while the length Y_4 affects both the first and second resonances. With $\mathrm{Y}_4 = 5.4\ \mathrm{mm}$ the two resonant frequencies decrease to 5.735 and 5.825 GHz and the antenna operating frequency is shifted back to 5.775 GHz with a further enhanced bandwidth of 90 MHz (5.725–5.815 GHz). Fig. 4(c) and (d) shows the simulated antenna radiation patterns in the E- and H-planes at 5.775 GHz, respectively. It is seen that the double-resonance technique does not alter the radiation patterns significantly. At 5.775 GHz the simulated antenna peak gain is 4.8 dBi and the radiation efficiency is 83%.

Authorized licensed use limited to: Nanyang Technological University. Downloaded on February 25,2010 at 22:03:30 EST from IEEE Xplore. Restrictions apply.

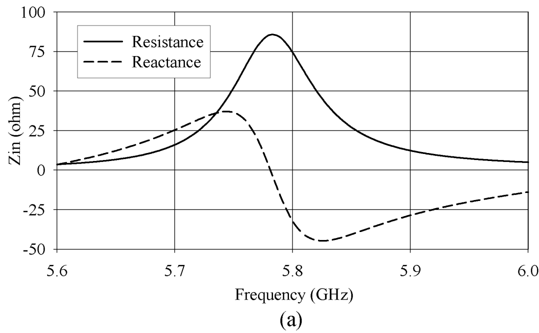

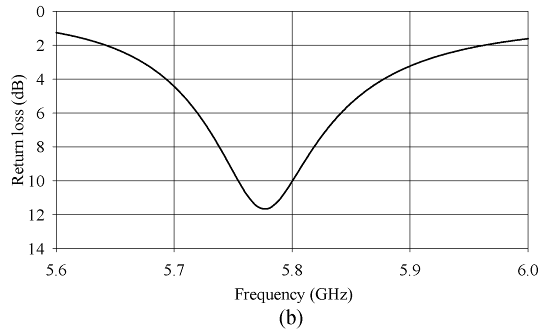

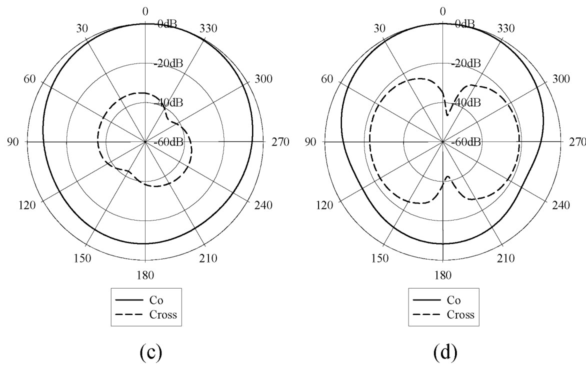

Fig. 2. Performance of the basic structure of the microstrip line antenna: (a) input impedance, (b) return loss, (c) E-plane patterns, and (d) H-plane patterns.

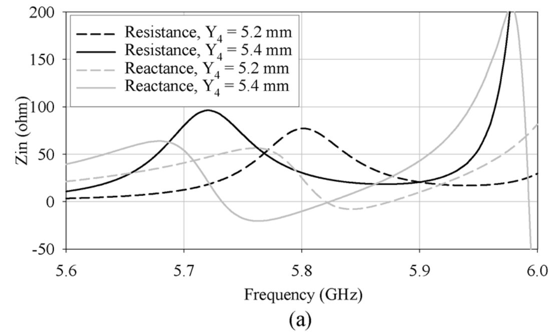

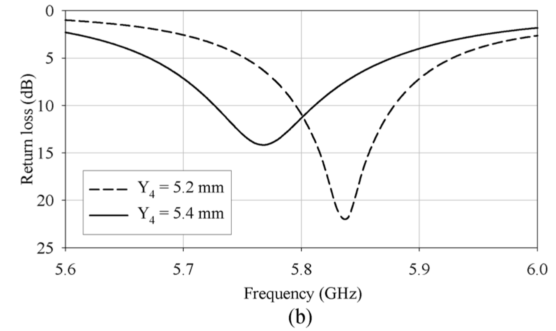

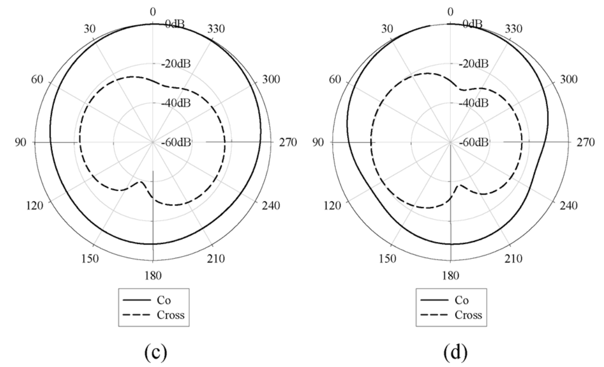

Fig. 4. Performance of the microstrip line antenna with a second current path: (a) input impedance, (b) return loss, (c) E-plane patterns ($\mathrm{Y}_4 = 5.4$ mm), and (d) H-plane patterns ($\mathrm{Y}_4 = 5.4$ mm).

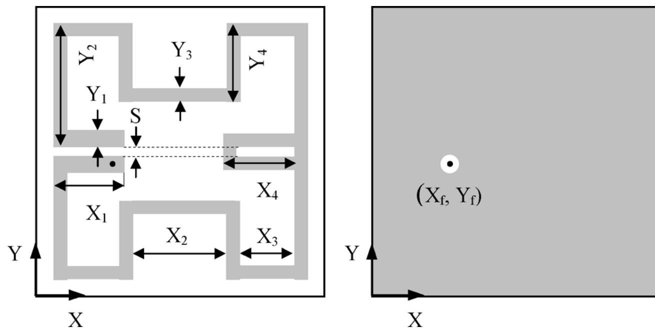

Fig. 3. Top and bottom views of the microstrip line antenna with a second current path.

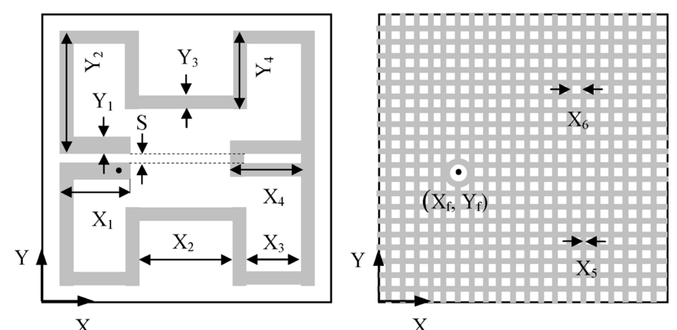

Fig. 5. Top and bottom views of the microstrip line antenna with a meshed ground plane.

C. Meshed Ground Plane

The meshed ground plane is required mainly from the mechanical perspective. However, its proper design can further enhance the antenna impedance bandwidth. Fig. 5 shows the microstrip line antenna and the meshed ground plane.

Using the design parameters listed in Table I, we simulated the antenna performance. It is observed from Fig. 6(a) that with the initial $\mathrm{Y}_4 = 5.4$ mm the double resonances are shifted down to 5.695 and 5.765 GHz as compared with 5.735 and 5.825 GHz in Fig. 4(a). The meshed ground plane perturbs the current return path and leads to the excitation of an electric field across the rectangular slots, and the reactive energy stored near the slot discontinuities is responsible for this downward frequency shift. In addition, the energy loss through the slots leads to the

Authorized licensed use limited to: Nanyang Technological University. Downloaded on February 25,2010 at 22:03:30 EST from IEEE Xplore. Restrictions apply.

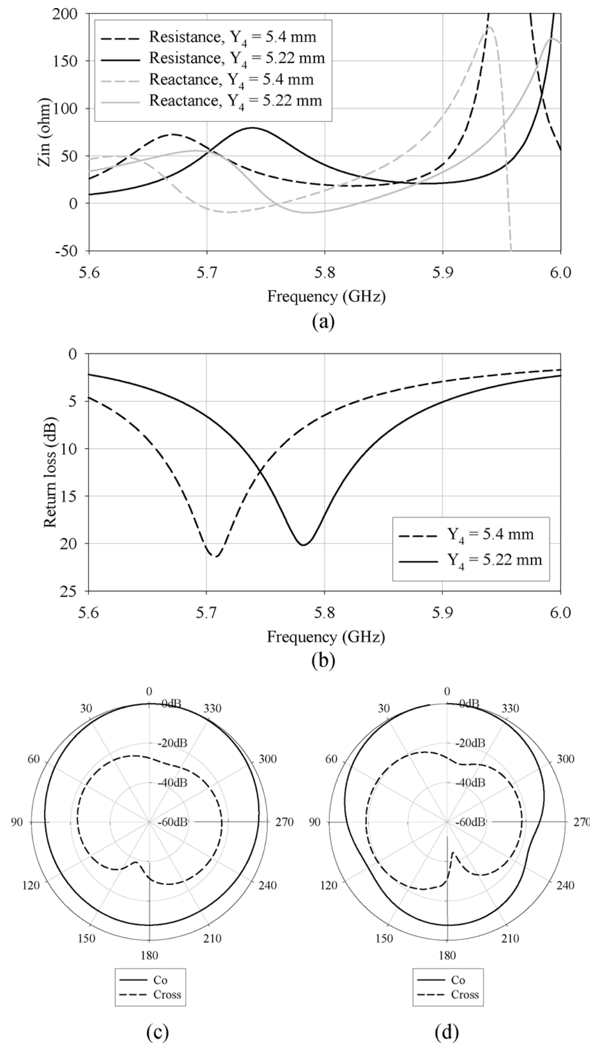

Fig. 6. Performance of the microstrip line antenna with a meshed ground plane: (a) input impedance, (b) return loss, (c) E-plane patterns ($Y_4 = 5.22\ \mathrm{mm}$), and (d) H-plane patterns ($Y_4 = 5.22\ \mathrm{mm}$).

reduction of the impedance values at and in the vicinity of the first resonant frequency, thus improving the matching performance. This is confirmed in Fig. 6(b) by an enhanced bandwidth of 110 MHz (5.655–5.765 GHz). However, the antenna operating frequency shifts away from 5.775 GHz again. It can be adjusted by decreasing the length Y_4. With $Y_4 = 5.22\ \mathrm{mm}$ the two resonant frequencies increases to 5.755 and 5.825 GHz and the antenna operating frequency is shifted back to 5.775 GHz with a bandwidth of 110 MHz (5.72–5.83 GHz), which satisfies the impedance bandwidth of 100 MHz for the standard. Fig. 6(c) and (d) shows the simulated antenna radiation patterns in the E- and H-planes at 5.775 GHz, respectively. It is seen that the meshed ground plane does not alter the radiation patterns significantly. The simulated antenna peak gain is 4.5 dBi and radiation efficiency is 81%. This optimized design will be used for further integration in Section III.

III. Integration of Microstrip Line Antenna in a Package

Fig. 7 shows the concept of integrating the microstrip line antenna in a package as an AiP. As shown, the AiP is in a cavity-down CBGA package format. Three ceramic layers are observed to form the package. Two buried metal layers are used for signal traces and the meshed ground plane, while the top metal layer is used for line radiating element of the antenna. Fig. 7 also shows a single-chip RF transceiver die attached upside down to the ground plane. This configuration will contribute to the shielding of the die from the antenna. Note that with a shared ground plane the shielding design has been greatly simplified. The single-chip RF transceiver die is connected to the external solder balls through the bond wires, traces, and vias. The die is also linked to the microstrip line antenna through three chains of bond wire, trace, and vias in a ground-signal-ground (GSG) fashion. This is known as an antenna feeding network in the AiP. Its design will be emphasized in this section because the package elements, in particular, the bond wire are rarely used for this application.

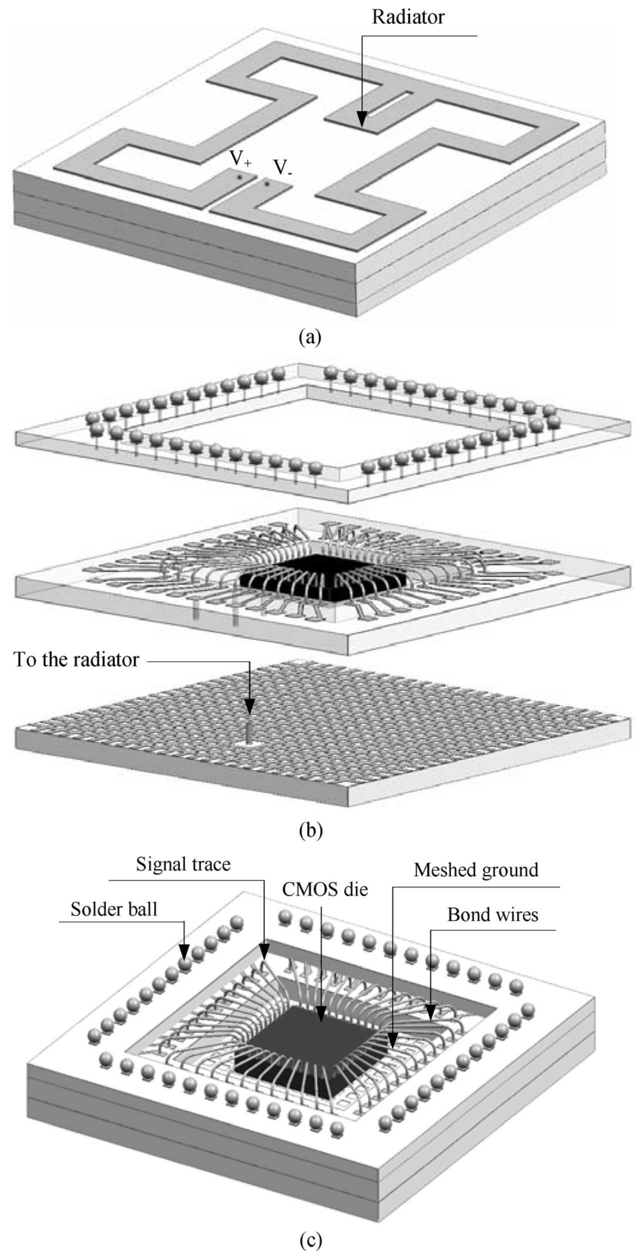

Fig. 7. The AiP: (a) top view, (b) explored view, and (c) bottom view.

Authorized licensed use limited to: Nanyang Technological University. Downloaded on February 25,2010 at 22:03:30 EST from IEEE Xplore. Restrictions apply.

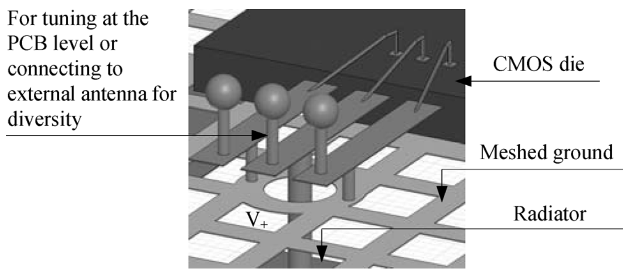

Fig. 8. The bond wire feeding network.

A. AiP Performance

Based on the concept described above, the microstrip line antenna has been integrated in a thin 64-ball CBGA package in LTCC. The CBGA package has dimensions of $17 \times 17 \times 1.6\ \mathrm{mm}^3$. For three layers shown in Fig. 7(b), the antenna layer uses the same geometry and dimensions as our microstrip line antenna in Section II-C, the trace and ball layers have the same thickness, and they form a stepped cavity large enough to hold a single-chip RF transceiver die. Fig. 8 shows the feeding network of the antenna from the RF transceiver die. The feeding network consists of such packaging elements as three bond wires cascaded first with three traces, and then three vias in a GSG arrangement. It is known that the GSG arrangement not only minimizes potential electromagnetic interference but also improves the feeding performance.

The design of the AiP feeding network is done according to our developed guidelines and steps. They are described as follows. A bond wire presents high impedance because of its high inductance and low capacitance. Thus, keeping the length of the bond wires to a minimum and using the bond wires with the largest possible diameter are critical to minimizing their disruptive influences on electrical signals. The GSG arrangement of bond wires improves the situation by providing a return path in close proximity to the wire and thus reducing inductance slightly. The signal and ground traces form a typical coplanar waveguide (CPW). The signal integrity is well preserved by this coplanar waveguide. However, there is some level of loss due to the dielectric material that is surrounding the traces. As such, the length of the trace section does have an influence on the overall electrical behaviour but is much less damaging than the bond wire. A via is a transition from a trace to the antenna through an aperture in or directly to the meshed ground plane. Vias are inductive. The aperture in the meshed ground plane allows the via to guide the signal to the antenna and therefore has the potential to impact it. The aperture is capacitive. The diameter of the aperture should be considered with the signal via.

Step 1) Given the size of the RF transceiver die and the wire bonding capability, the diameter, loop height, and length of the bond wire are determined. Typically, the bond wire for RF applications is gold and has a diameter of 25.4 or 32.5 $\mu\mathrm{m}$, a loop height from 0.1 to 0.2 mm, and the length from 0.8 to 1.2 mm.

Step 2) Based on step 1, the cavity size is determined and so are the lengths of the traces. The width and gap of the traces are estimated for a 50-Ω CPW line using empirical formula or the free computer-aided design software, TXLine.

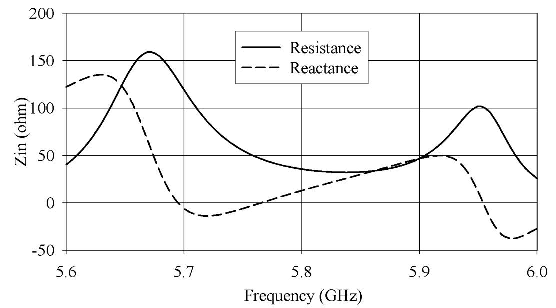

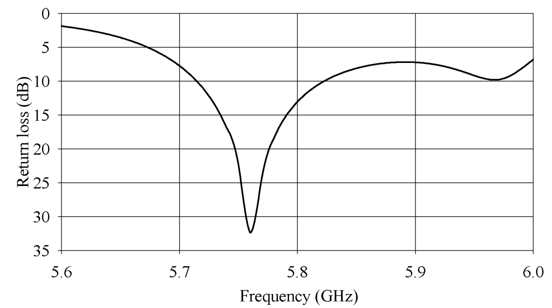

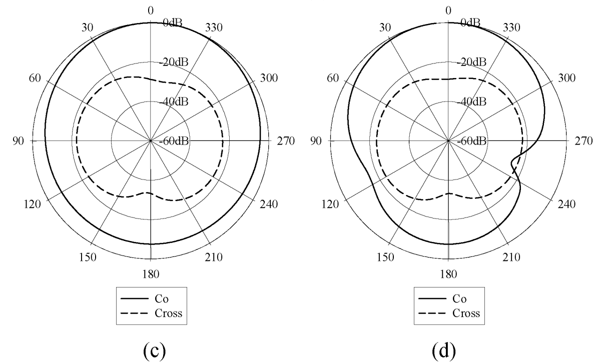

Fig. 9. Performance of the AiP: (a) input impedance, (b) return loss, (c) E-plane patterns, and (d) H-plane patterns.

Step 3) Limited by the LTCC process, only a few via diameters are possible. They are 0.1, 0.15, and 0.2 mm. The larger diameter is preferable for a longer via. Once the via diameter is determined, the aperture diameter can be estimated for a 50-Ω coaxial line using empirical formula.

Step 4) Optimize the cascaded packaging elements of bond wires, traces, and vias in the HFSS until the best matching performance for the AiP at the operating frequency has been achieved within the LTCC physical layout rules.

Fig. 9 shows the simulated performance of the AiP designed for a single-chip RF transceiver die of typical size $6 \times 6 \times 0.4\ \mathrm{mm}^3$. The AiP contains a stepped cavity of size $(8.5 \times 8.5 + 6.5 \times 6.5) \times 0.4\ \mathrm{mm}^3$. The bond wire has a diameter of 32.5 $\mu\mathrm{m}$, a loop height of 0.2 mm and a length of 1 mm. The traces have a width of 0.32 mm, a gap of 0.16 mm, and a length of 2 mm. The signal via has a diameter of 0.2 mm, the aperture has a diameter of 0.6 mm, and the ground via has a diameter of 0.1 mm. Fig. 9(a) shows that the double resonances still occur in the 802.11a frequency band. Fig. 9(b) shows that the AiP impedance bandwidth remains the same

Authorized licensed use limited to: Nanyang Technological University. Downloaded on February 25,2010 at 22:03:30 EST from IEEE Xplore. Restrictions apply.

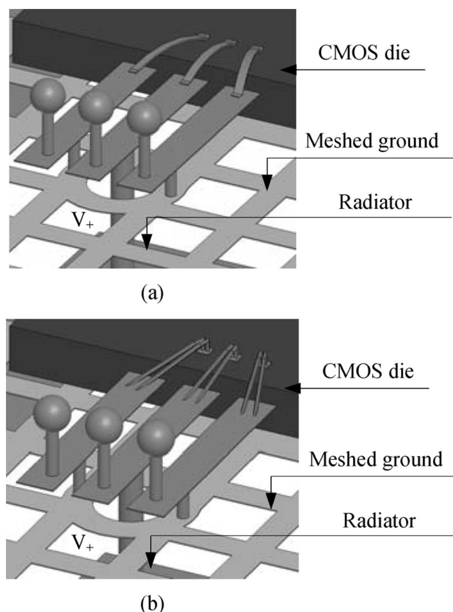

Fig. 10. The advanced bond wire feeding network: (a) ribbon and (b) double wire.

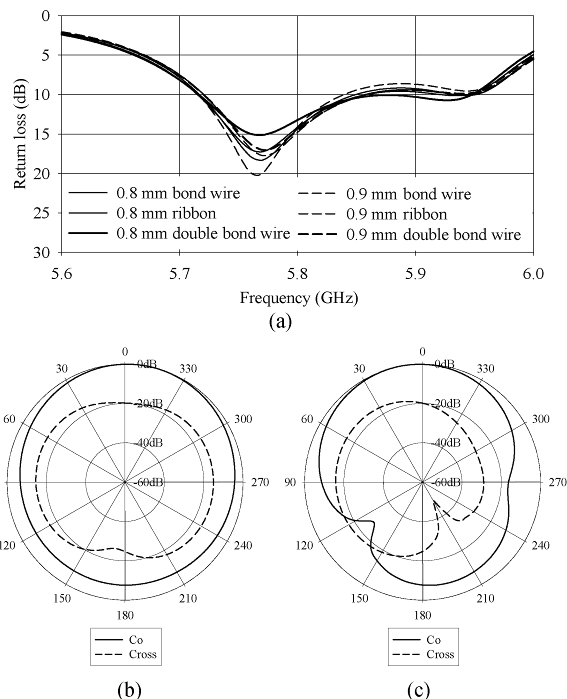

Fig. 11. Enhanced performance of the AiP using advanced bonding techniques: (a) return loss, (b) E-plane patterns (0.8-mm double bond wire), and (c) H-plane patterns (0.8-mm double bond wire).

as that of the microstrip line antenna, that is, 110 MHz from 5.72 to 5.83 GHz, which satisfies the impedance bandwidth of 100 MHz for the standard. Fig. 9(c) and (d) show the simulated AiP radiation patterns in the E- and H-planes at 5.775 GHz, respectively. It is seen that the integration does not alter the radiation patterns significantly. They are comparable with un-integrated counterparts of Fig. 6. In addition, the simulated AiP peak gain and radiation efficiency are 4.6 dBi and 85%, respectively. Comparing this extracted efficiency with that in Section II-C their difference seems not very relevant due to the limited accuracy of the EM simulator.

B. Enhanced AiP Performance

It is seen from Fig. 9(a) that beside the first and second resonances which contribute to the wide bandwidth, there is a third resonance at 5.95 GHz. This enlightens us to further enhance the AiP impedance bandwidth. As shown decreasing the inductance will result in a better matching for the frequency band between the second and third resonance. From the feeding network as analyzed, the bond wire contributes mainly to the high inductance. Here, the loop height of the bond wire is decreased to 0.1 mm. Its length is decreased to 0.8 and 0.9 mm to minimize its disruptive influence on the electrical signal. As expected, the matching performance between the second and third resonance frequencies improves greatly in Fig. 11(a), which leads to an acceptable 9-dB bandwidth of 250 MHz from 5.71 to 5.96 GHz for the bond wire of 0.8 mm long. In addition, it is possible to use the advanced ribbon or double bond wire techniques as shown in Fig. 10 to decrease the inductance. The ribbon is mainly used for packaging devices or modules at microwave and millimeter-wave frequencies. The double bond wire technique is more effective, reliable and cost-effective for the frequencies interested here. The gold ribbons used here are 76 μm wide, 12.7 μm thick and 76 μm high. The double bond wires used here have a diameter of 32.5 μm and a loop height of 0.1 mm. Their lengths vary from 0.8 and 0.9 mm. As shown in Fig. 11(a) the characteristics of the double bond wires are similar to that of the ribbon in decreasing the inductance and thus enhancing the bandwidth. The best performance is achieved by the 0.8-mm double bond wire case. The 10-dB impedance bandwidth is 230 MHz from 5.715 to 5.945 GHz. Fig. 11(b) and (c) also shows the simulated radiation patterns in the E- and H-planes at 5.9 GHz, respectively. In addition, the simulated peak gain and radiation efficiency are 4.75 dBi and 85%, respectively.

It should be mentioned that the AiP performance enhancement by only changing bonding techniques is very limited. As seen in Fig. 11(a) the input match is almost the same for single wire, double wire, and ribbon bonding. The slight match improvement at some frequencies was achieved at the worse match at lower frequencies. In addition, in the real fabrication decreasing the bond wire or ribbon length to a minimum affects the yield. Thus, global optimization of the AiP is necessary. As shown in Section II the length X_4 can shift the second resonance effectively but no influence on the first resonance. For our designed AiP in Section III-A the bandwidth can also be enhanced by only increasing X_4. As shown in Fig. 12, the 10-dB impedance bandwidth of 210 MHz from 5.715 to 5.925 GHz is achieved for $X_4 = 4.6$ mm and of 200 MHz from 5.715 to 5.915 GHz for $X_4 = 4.7$ mm. Fig. 12(b) and (c) also shows the simulated radiation patterns in the E- and H-planes at 5.9 GHz, respectively for the case of $X_4 = 4.7$ mm. In addition, the simulated peak gain and radiation efficiency are 4.57 dBi and 85%, respectively.

IV. Modification of AiP for Differential Architecture

A differential architecture is of great advantage in current silicon technology for single-chip RF transceivers because the differential nature permits higher linearity, lower offset, and

Authorized licensed use limited to: Nanyang Technological University. Downloaded on February 25,2010 at 22:03:30 EST from IEEE Xplore. Restrictions apply.

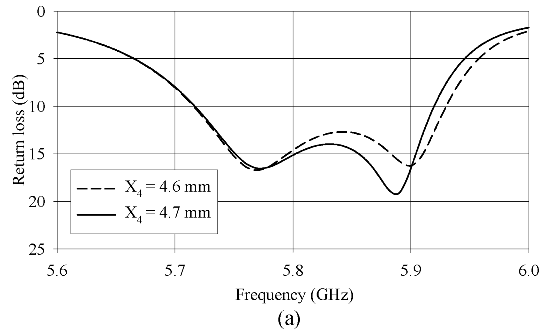

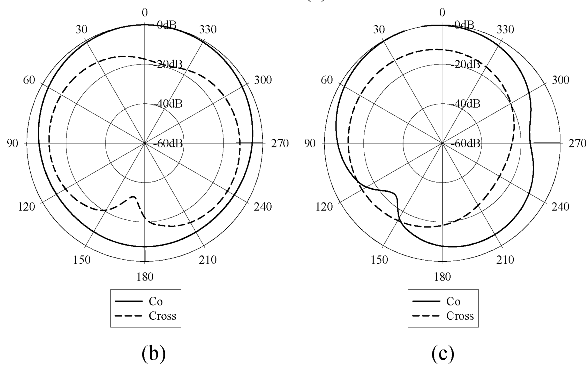

Fig. 12. Enhanced performance of the AiP by a global optimization: (a) return loss, (b) E-plane patterns ($X_4 = 4.7$ mm), and (c) H-plane patterns ($X_4 = 4.7$ mm).

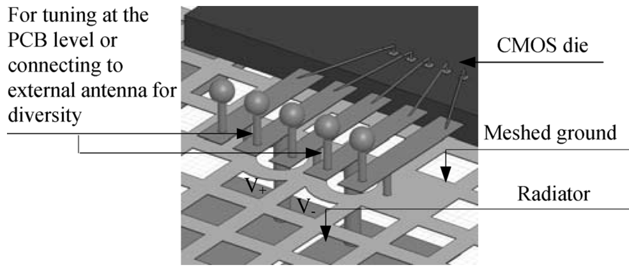

Fig. 13. The feeding network for the differential AiP.

makes it immune to power supply variations and substrate noise. Thus, exploring the design of differential AiP is essential for these transceivers to get rid of bulky off-chip or lossy on-chip baluns. With a symmetrical structure of the radiating element of the microstrip line antenna, a differential AiP can be easily realized. The differential AiP is realized by modifying the ground plane and adding another feeding network. Thus, the differential AiP is actually a meandered loop antenna. Fig. 13 shows the designed feeding network for the differential AiP. The feeding network consists of such packaging elements as five bond wires cascaded first with five traces, and then five vias in a GSGSG fashion. The signal trace is 0.32 mm wide. The central ground trace is 0.3 mm wide. The outside ground trace is 0.35 mm wide. These traces are all 2 mm long with a gap of 0.16 mm between adjacent traces. Gold bond wires are used here with a diameter of 32.5 μm, a loop height of 0.1 mm, and the length of 1 mm. For the differential AiP, the input impedance Z_d is calculated using two-port Z-parameters as $Z_d = 2\,(Z_{11} - Z_{21}) = 2\,(Z_{22} - Z_{12})$. The Z-parameters are obtained with differential excitation at the CMOS die wire

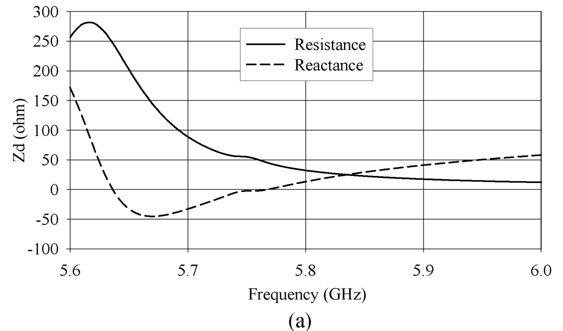

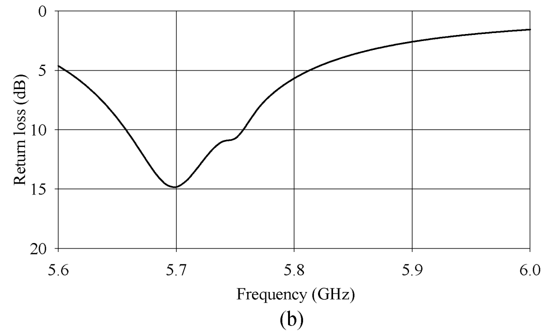

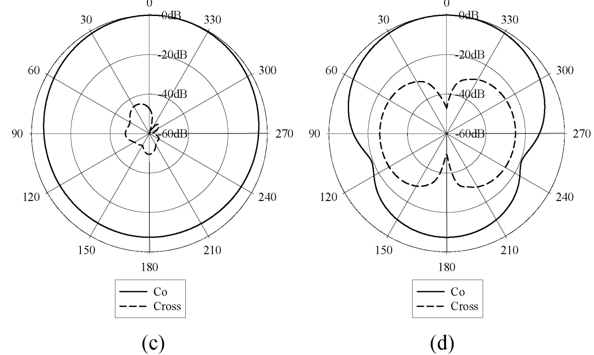

Fig. 14. Performance of the differential AiP: (a) input impedance, (b) return loss, (c) E-plane patterns at 5.7 GHz, and (d) H-plane patterns at 5.7 GHz.

bonding pads as shown in Fig. 13. The return loss is given by $RL = 20\log|(Z_d - Z_0)/(Z_d + Z_0)|$ where Z_0 is 100 Ω. Fig. 14 shows the simulated performance of the differential AiP. It is seen from Fig. 14(a) and (b) that the double resonances still occur and the bandwidth of 100 MHz still satisfies the standard. However, the AiP operating frequency shifts down to 5.7 GHz. The AiP operating frequency can be adjusted to 5.775 GHz by decreasing the length of the line radiating element. Fig. 14(c) and (d) shows that the differential AiP has much lower cross-polar radiation particularly in the E-plane. The lower cross-polar radiation is the result of symmetrical structure and excitation. The simulated differential AiP has a peak gain of 4.7 dBi and a radiation efficiency of 85%.

V. Experimental Results

The AiP designs were fabricated in DuPont LTCC. They include the single-ended AiP designed in Section III-A and the differential AiP designed in Section IV. Nine samples were made for both types, each. They were surface mounted on PCBs for testing. The size of each PCB was $60 \times 40 \times 0.8$ mm^3. An Agilent network analyzer E5062A was used to measure the

Authorized licensed use limited to: Nanyang Technological University. Downloaded on February 25,2010 at 22:03:30 EST from IEEE Xplore. Restrictions apply.

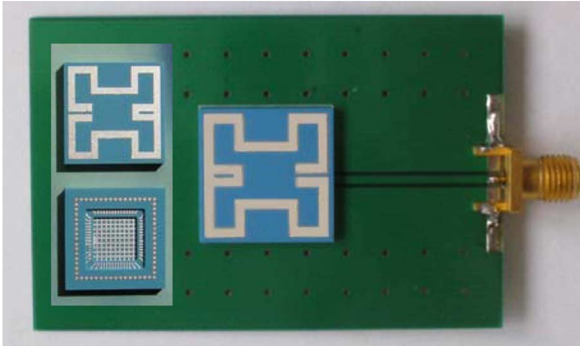

Fig. 15. Photos of single-ended AiP and the mounting for testing. The CPW ground plane is removed under the AiP.

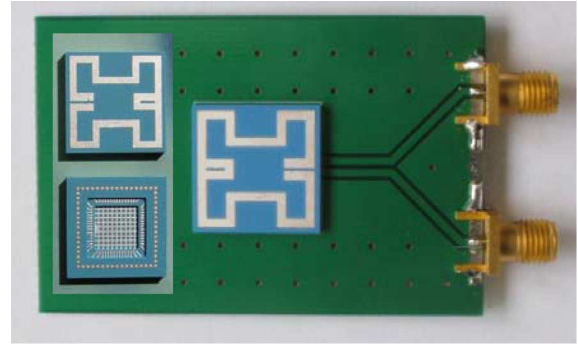

Fig. 17. Photos of differential AiP and the mounting for testing. The CPW ground plane is removed under the AiP.

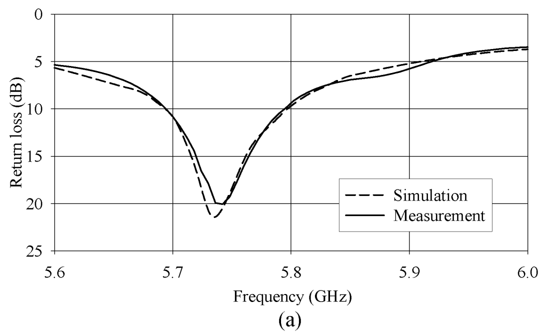

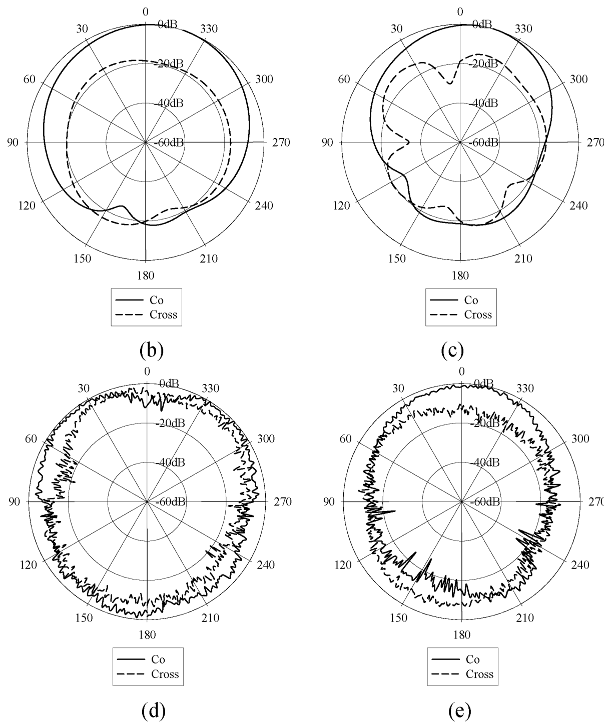

Fig. 16. Performance of the single-ended AiP ($X_4 = 4.2$ mm, $Y_4 = 5.22$ mm): (a) simulated and measured return losses, (b) simulated E-plane patterns, and (c) simulated H-plane patterns, (d) measured E-plane patterns, and (e) measured H-plane patterns.

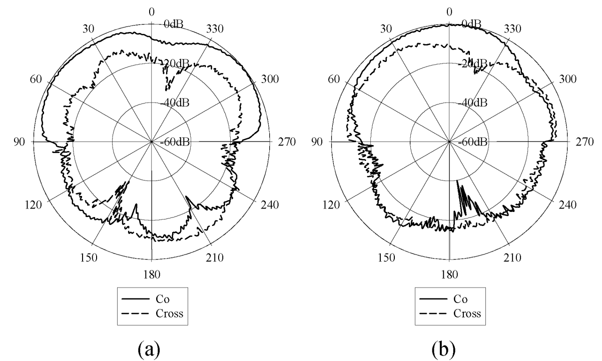

Fig. 18. Measured performance of the differential AiP: (a) E-plane patterns at 5.6 GHz, and (b) H-plane patterns at 5.6 GHz.

S_{11}, and an HP 8510C network analyzer was used to measure the radiation patterns and gain in an anechoic chamber. Due to the lack of facilities to truly measure an AiP for differential signal operation, the differential AiP was measured by using a balun that forces opposite currents in each feed of the AiP. The balun was a J-212-180 from ET Industries at Boonton, NJ.

A. Single-Ended AiP

Fig. 15 shows the photos of the top and bottom views of the single-ended AiP and the mounting for testing. The RF signal was guided by the CPW on the PCB, the vias in the bottom layer of the AiP (see the vias for tuning at the PCB level and for connecting to the external antenna for diversity in Fig. 8), the traces that were partially embedded between the bottom and middle layers of the AiP, and the vias of which two were grounded and one was led though the aperture in the meshed ground plane of the AiP to feed the radiating element. The model of the AiP mounted on the PCB is simplified and simulated. The solder balls, signal traces, bond wires, and PCB vias that are not in or in the vicinity of the feeding network are removed except for some ones for keeping signal and ground integrity.

B. Differential AiP

Fig. 17 shows photos of the top and bottom views of the differential AiP and the mounting for testing. The differential RF signal was guided by the two transmission lines on the PCB, the vias in the bottom layer of the AiP (see the vias for tuning at the PCB level and for connecting to the external antenna for diversity in Fig. 13), the traces that were partially embedded between the bottom and middle layers of the AiP, and the vias of which three were grounded and two were led though the two apertures

Authorized licensed use limited to: Nanyang Technological University. Downloaded on February 25,2010 at 22:03:30 EST from IEEE Xplore. Restrictions apply.

in the meshed ground plane of the AiP to feed the radiating element. The measured center frequency is 5.6 GHz. Because the influence of balun can not be de-embedded, no return loss and bandwidth details are provided here. Fig. 18 shows the measured radiation patterns. As expected, the cross-polar radiation particularly in the E-plane is much lower than that of the single-ended AiP. No simulation was run as details of the balun were unknown. Nevertheless, the measured results demonstrate the feasibility of the AiP for differential operation. The simulated and measured return losses are plotted in Fig. 16(a). The measured impedance bandwidth is 102 MHz ($102/5742 \approx 1.8\%$) and the simulated impedance bandwidth is 100 MHz ($100/5732 \approx 1.7\%$). The slight discrepancy between the measured and simulated return losses may be caused by fabrication tolerances in the LTCC shrinkage control. The simulated radiation patterns at 5.742 GHz are plotted in Fig. 16(b) and (c) for the E- and H-planes, respectively; while the measured radiation patterns at 5.742 GHz are plotted in Fig. 16(d) and (e) for the E- and H-planes, respectively. It is seen that there are differences between the simulated and measured radiation patterns. These differences may be due to limitation in HFSS. For example, the influence of the TM_0-mode surface wave that shifts the strongest radiation from the broadside direction in the E plane can be observed in the measured but not in the simulated radiation patterns. The differences can also be attributed to the traces and vias that were not used in the feeding network but would be used in integration of the AiP with the single-chip RF transceiver die. These non-feeding traces and vias were not included in the simulation. The peak gain was measured to be 3.0 dBi, which was about 1.5 dB lower than the simulated gain. The difference was related to the polarization purity. The polarization purity affects the linearly-polarized gain. The simulated polarization purity was much better than the measured one. The poor measured polarization purity might be caused by the radiation influence from the feed connector added to the resulted radiation pattern of the actual antenna structure. Also, there was an estimated uncertainty ± 1 dB from the calibration of the transmission loss of the CPW on the PCB and the data sheet of the horn antenna. The efficiency was not measured but verified with another simulation tool Microwave Studio from CST at Darmstadt, Germany, which showed the efficiency to be also about 80%. Nevertheless, the measured results basically verify the performance of the AiP design.

VI. Conclusion

A novel AiP design in LTCC technology for single-chip RF transceivers operating in the 5-GHz band was presented. First, the design of a basic microstrip line antenna on an LTCC substrate was described. Then, a double-resonance technique and meshed ground plane were proposed to enhance its impedance bandwidth. Next, the microstrip line antenna was integrated into the novel AiP with emphasis on feeding the microstrip line antenna using the packaging elements from the carried single-chip RF transceiver die. After that, the bandwidth enhancement techniques for the AiP were developed. This was followed by modifying the AiP to support the operation of differential signal to suit the mainstream design of single-chip RF transceivers in a differential architecture. Finally, the performance of the AiP design was measured and verified. It is therefore anticipated that the design details and results on the AiP are useful and inspiring for those interested in novel antenna solutions for modern RF transceivers for wireless communications.

Acknowledgment

The authors would like to thank their former group members Mr. Y. Xue, Mr. L. H. Xiao, Mr. S. H. Wi, and Mr. D. A. V. Thanh for their assistance in this work.

References

[1] A. R. Behzad, M. S. Zhong, S. B. Anand, L. Li, K. A. Carter, M. S. Kappes, T. H. Lin, T. Nguyen, D. Yuan, S. Wu, Y. C. Wong, V. Gong, and A. Rofougaran, "A 5-GHz direct-conversion CMOS transceiver utilizing automatic frequency control for the IEEE 802.11a wireless LAN standard," *IEEE J. Solid-State Circuits*, vol. 38, no. 12, pp. 2209–2220, 2003.

[2] T. P. Liu and E. Westerwick, "5-GHz CMOS radio transceiver front-end chipset," *IEEE J. Solid-State Circuits*, vol. 35, no. 12, pp. 1927–1933, 2003.

[3] [Online]. Available: http://www.ntktech.com/Antenna/Antenna_PDF/

[4] [Online]. Available: http://www.trda-inc.com/

[5] Y. Hwang, Y. P. Zhang, G. X. Zheng, and T. K. C. Lo, "Planar inverted F antenna loaded with high permittivity material," *Electron. Lett.*, vol. 31, no. 20, pp. 1710–1712, 1995.

[6] [Online]. Available: http://www.ltcc.de

[7] Y. P. Zhang, "Integration of microstrip antenna on ceramic ball grid array package," *Electron. Lett.*, vol. 38, no. 1, pp. 14–16, 2002.

[8] Y. P. Zhang, "Finite-difference time-domain analysis of an integrated circuit ceramic ball grid array package antenna for single-chip wireless transceivers," *IEEE Trans. Antennas Propag.*, vol. 52, pp. 435–442, Feb. 2004.

[9] Y. P. Zhang, "Integrated ceramic ball grid array package antenna," *IEEE Trans. Antennas Propag.*, vol. 52, pp. 2538–2544, 2004.

[10] C. C. Zhang, J. J. Liu, and Y. P. Zhang, "ICPA for highly integrated concurrent dual-band wireless receivers," *Electron. Lett.*, vol. 39, no. 12, pp. 887–889, 2003.

[11] J. J. Wang, Y. P. Zhang, C. W. Lu, and K. M. Chua, "Circuit model of microstrip patch antenna on ceramic land grid array package for antenna-chip codesign of highly integrated RF transceivers," *IEEE Trans. Antennas Propag.*, vol. 53, pp. 3877–3883, Dec. 2005.

[12] W. Wang and Y. P. Zhang, "0.18-μm CMOS push-pull power amplifier with antenna in IC package," *IEEE Microw. Wireless Compon. Lett.*, vol. 14, pp. 13–15, Jan. 2004.

[13] Y. P. Zhang, "Antenna-in-package (AiP) technology for modern radio systems," presented at the IEEE Workshop on Antenna Technology, New York, Mar. 6–8, 2006.

[14] Z. H. Lu, C. L. Tang, and S. H. Yeh, "Antenna in package scheme," (in Chinese) *CCL Tech. J.*, vol. 102, pp. 70–75, Dec. 2005.

[15] C. W. Ling, C. Y. Lee, C. L. Tang, and S. J. Chung, "Analysis and application of an on-package planar inverted-F antenna," *IEEE Trans. Antennas Propag.*, vol. 55, pp. 1774–1780, Jun. 2007.

[16] R. R. Tummala *et al.*, "The SOP for miniaturized, mixed-signal computing, communication, and consumer systems of the next decade," *IEEE Trans. Adv. Packag.*, vol. 27, pp. 250–267, 2004.

[17] S. B. Brebels *et al.*, "SOP integration and codesign of antennas," *IEEE Trans. Adv. Packag.*, vol. 27, pp. 341–351, 2004.

[18] S. H. Wi *et al.*, "Package-level integrated antennas based on LTCC technology," *IEEE Trans. Antennas Propag.*, vol. 54, pp. 2190–2197, Aug. 2006.

[19] C. T. P. Song, P. S. Hall, and H. Ghafouri-Shiraz, "Novel RF front end antenna package," *Proc. Inst. Elect. Eng. Microw. Antennas Propag.*, vol. 150, no. 4, pp. 290–294, Aug. 2003.

[20] E. H. Lim and K. W. Leung, "Novel application of the hollow dielectric resonator antenna as a packaging cover," *IEEE Trans. Antennas Propag.*, vol. 54, pp. 484–487, 2006.

[21] T. C. Edwards, *Foundations for Microstrip Circuit Design*. New York: Wiley, 1981.

Authorized licensed use limited to: Nanyang Technological University. Downloaded on February 25,2010 at 22:03:30 EST from IEEE Xplore. Restrictions apply.

Y. P. Zhang received the B.E. and M.E. degrees from Taiyuan Polytechnic Institute and Shanxi Mining Institute of Taiyuan University of Technology, Shanxi, China, in 1982 and 1987, respectively and the Ph.D. degree from the Chinese University of Hong Kong, Hong Kong, in 1995, all in electronic engineering.

From 1982 to 1984, he worked at Shanxi Electronic Industry Bureau, from 1990 to 1992, the University of Liverpool, Liverpool, U. K., and from 1996 to 1997, City University of Hong Kong. From 1987 to 1990, he taught at Shanxi Mining Institute and from 1997 to 1998, the University of Hong Kong. He was promoted to a Full Professor at Taiyuan University of Technology in 1996. He is now an Associate Professor and the Deputy Supervisor of Integrated Circuits and Systems Laboratories with the School of Electrical and Electronic Engineering, Nanyang Technological University, Singapore. He has broad interests in radio science and technology and published widely across seven IEEE societies. He has delivered scores of invited papers/keynote address at international scientific conferences.

Dr. Zhang received the Sino-British Technical Collaboration Award in 1990 for his contribution to the advancement of subsurface radio science and technology. He received the Best Paper Award from the Second International Symposium on Communication Systems, Networks and Digital Signal Processing, July 2000, Bournemouth, U.K., and the Best Paper Prize from the Third IEEE International Workshop on Antenna Technology, March 2007, Cambridge, U.K. He was awarded a William Mong Visiting Fellowship from the University of Hong Kong in 2005. He has organized/chaired dozens of technical sessions of international symposia. He is listed in *Marquis Who's Who, Marquis Who's Who in Science and Engineering,* and *Outstanding Scientists of the 21st Century, Cambridge IBC 2000*. He serves on the Editorial Boards of the IEEE TRANSACTIONS ON MICROWAVE THEORY AND TECHNIQUES, IEEE MICROWAVE AND WIRELESS COMPONENTS LETTERS, the *International Journal of RF and Microwave Computer-Aided Engineering* and was a Guest Editor of the journal's Special Issue RF and Microwave Subsystem Modules for Wireless Communications. He also serves as an Associate Editor of the *International Journal of Microwave Science and Technology*.

M. Sun received the B.E. and M.E. degrees from the Hunan University and Beijing Institute of Technology, China, in 2000 and 2003, respectively, and the Ph.D. degree from the Nanyang Technological University (NTU), Singapore, in 2007, all in electronic engineering.

She became a Research Associate in NTU in 2006 and subsequently converted to Research Fellow in 2007. Her research interests include intra- and inter-chip RF wireless communication system simulation and implementation, and integrated antenna design for wireless communication.

Dr. Sun was a recipient of the Best Paper Prize from the IEEE 3rd International Workshop on Antenna Technology, March 2007, Cambridge, U.K.

W. Lin received the B.E. degree in automation engineering from Qingdao University, China, in 1991 and the M.E. degree in electronic engineering from Nanyang Technological University, Singapore, in 2004.

From 2000 to 2003, he worked at Chartered Semiconductor Manufacturing (CSM) Ltd., Singapore, and from 2004 to 2006, Centurion Electronics (Shanghai) Ltd., China. He is a co-founder of the Shanghai Fretune Communication Technology Ltd., China. Since 2006, he has been a Manager with this company leading the antenna design team.

Authorized licensed use limited to: Nanyang Technological University. Downloaded on February 25,2010 at 22:03:30 EST from IEEE Xplore. Restrictions apply.